Journal of Applied Polymer Science

Fabrication and characterization of hybrid films based on polyaniline and graphitic carbon nitride nanosheet

Mohammad Dinari, Mohamad Mohsen Momeni, Mohaddeseh Afshari
Department of Chemistry, Isfahan University of Technology, Isfahan 84156-83111, Iran
Correspondence to: M. Dinari (E-mail: dinari@cc.iut.ac.ir; mdinary@gmail.com); M. M. Momeni (E-mail: mm.momeni@cc.iut.ac.ir)

ABSTRACT: Hybrid films of polyaniline/graphitic carbon nitride (PANI/g-C_3N_4) deposited on titanium was fabricated. First, g-C_3N_4 as a two-dimensional graphite-like structure was synthesized by the stepwise condensation reaction of melamine and cyanuric chloride in the presence of *N*,*N*-dimethylmethanamide as a high boiling point nonnucleophilic base. Then composite films of PANI/g-C_3N_4 were prepared by *in situ* electrochemical polymerization of an aniline solution containing g-C_3N_4. Different concentrations of g-C_3N_4 were utilized to improve the electrochemical performances of the hybrids. The resulting PANI/g-C_3N_4 composite films were characterized by X-ray diffraction, field emission scanning electron microscopy, transmission electron microscopy, Fourier transform infrared spectroscopy, and ultraviolet–visible diffuse reflection spectroscopy techniques. The electrochemical performance of the composites was evaluated by cyclic voltammetry (CV). Application of the prepared samples has been evaluated as supercapacitor material in 0.5 *M* H_2SO_4 solution using CV technique. The specific capacitances of PANI/g-C_3N_4 composite films were higher than obtained for pure PANI films. © 2016 Wiley Periodicals, Inc. J. Appl. Polym. Sci. **2016**, *133*, 44059.

KEYWORDS: applications; conducting polymers; electrochemistry; films

Received 30 March 2016; accepted 13 June 2016
DOI: 10.1002/app.44059

INTRODUCTION

One of the great challenges in the 21st century is unquestionably energy storage. In this sense, we need novel economical and environmentally benign energy conversion and storage systems.[1] So, a strong demand for the development of inexpensive, flexible, light-weight, and green energy storage devices is necessary.[2,3] As an intermediate system between dielectric capacitors and batteries, supercapacitors are emerging as efficient energy storage devices due to their fast charge/discharge capability, high power density, long-term stability, and broad energy storage application prospects.[4,5] Supercapacitors have several applications in different areas, including power electronics, memory protection, battery enhancement, portable energy sources, power quality improvement, adjust able speed drives, high power actuators, hybrid electric vehicles, renewable and off-peak energy storage, and military and aerospace applications.[6–8] Recently, much effort has been devoted to developing the nanostructure and good conductive electrode materials that has high electrochemical capacitance.[9,10] Though it is still a critical challenge to enhance the energy density and cycling stability while retain the high-power density of electrode materials for flexible supercapacitors,[10,11] conducting polymers, carbon-based materials, and metal oxides have been extensively used for high performance electrode materials.[12–14]

Various conducting polymers have been reported for supercapacitor application, and the majority of research works reported till date is based on polyaniline (PANI), due to its reasonably high specific capacitance, high stability, light weight, and low material cost.[15,16] It holds great promise than other conducting polymers due to its unique tunable conductivity either by protonation or by charge-transfer doping. Due to its conducting behavior and thermal stability, it has been widely used in electrocatalysis, electrochromic devices, and biosensors.[17,18] Though PANI has several advantages like high polymerization yield, good redox reversibility, and high thermal and environmental stability, yet it shows its conductivity only in acidic media at pH < 3 in Emeraldine salt state.[19] However, the poor stability during the charge/discharge process restricts its practical applications in supercapacitor.[20,21] In order to maximize the electrochemical performance, the nanostructure PANI is greatly developed.

Graphitic carbon nitride (g-C_3N_4), a two-dimensional graphite-like structure, exhibited strong attraction owing to its high nitrogen content, excellent chemical and thermal stability, special optical features, appealing electronic structure, and environmental friendly feature.[22–25] Due to the high nitrogen content, g-C_3N_4 may provide more active reaction sites than other *N*-carbon materials to serve as a feasible template for metal

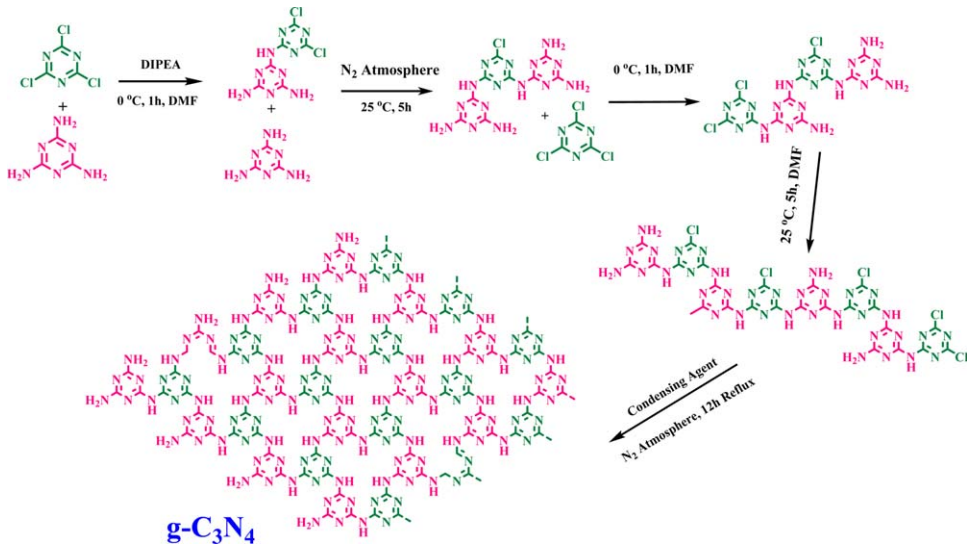

Scheme 1. Condensation reactions of melamine and cyanuric chloride to produce extended networks of g-C_3N_4. [Color figure can be viewed in the online issue, which is available at wileyonlinelibrary.com.]

nucleating as well as growing.[26] Moreover, g-C_3N_4 is often well-crystallized due to the nature of the lamellar structure, which consequently facilitates the charge transfer as well. Compared with graphene, g-C_3N_4 can be easily synthesized by polycondensation directly without any complicated post treatment. Also, the presence of nitrogen in g-C_3N_4 may provide more active reaction sites, increase the electron donor/acceptor characteristics, improve the wettability with the electrolytes and consequently enhance the mass transfer efficiency, and provide a large additional pseudocapacitance.[27,28] g-C_3N_4 has exhibited multifunctional potential applications in the fields of CO_2 reduction, hydrogen/oxygen evolution through water splitting, wastewater detoxification, electroactive materials for batteries, sensor, and so on.[29–32]

In recent years, there have been many reports about the preparation of g-C_3N_4/metal oxides hybrids. However, the g-C_3N_4 composites were mainly focused on photocatalysis applications,[33–36] and to the best of our knowledge, coupling of PANI and g-C_3N_4 as the electrode materials for supercapacitors has not been reported yet. In this study, for the first time, a PANI/g-C_3N_4 composite film was synthesized by *in situ* electropolymerization of aniline monomer in the presence of g-C_3N_4 powder on titanium electrode. Chemical structure and morphology of PANI/g-C_3N_4 composite films and electrochemical performances as electrode materials for supercapacitors were investigated. Comparison of the supercapacitive properties of the PANI sample with the composite material demonstrated significant improved specific capacitance.

EXPERIMENTAL

Chemicals, Solutions, and Equipment

All chemicals were of analytical grade purity. Aniline was distilled under reduced pressure and then stored at low temperature before use. Melamine and cyanuric chloride were parches from Merck Chemical CO (NJ, USA).

All electrochemical experiments were carried out at room temperature. Distilled water was used throughout this study. The electrochemical experiments were performed in a three-electrode cell assembly. A platinum sheet was used as counter electrode, while all potentials were measured with respect to a commercial saturated calomel electrode. Electrochemical experiments were carried out using a computerized potentiostat/galvanostat SAMA 500 (Isfahan, Iran).

Synthesis of g-C_3N_4

g-C_3N_4 was synthesized by the stepwise condensation reaction of melamine and cyanuric chloride. In brief, 0.1 g (1 mmol) of melamine was dispersed in 50 mL of DMF under stirrer at 0 °C, and then 0.146 g (1 mmol) of cyanuric chloride was added to the suspension. After 10 min, few drops of diisopropyleethylamine were poured into the mixture, and it was stirred for 1 h. Then the reaction temperature was increased to room temperature, and the solution was stirred for an additional 6 h under N_2 atmosphere. In the next step, the temperature was reduced to 0 °C, 1 mmol of cyanuric chloride was added to the reaction mixture, and it was stirred for 1 h. Then, the reaction temperature was raised to 25 °C for 5 h. Finally, it was refluxed for 12 h under nitrogen. After cooling, the precipitates was collected by filtration, and it was washed with a solution of 3:3:4 of benzene:hexane:water. The resulting product was washed with DMF by Soxhlet extractor and then dried under vacuum at 100 °C.

Preparation of PAN/g-C_3N_4/Ti Electrodes

Electropolymerization of PANI from an acidic solution was conducted on titanium electrode. Titanium discs were cut from a titanium sheet (purity 99.99%, 1 mm thickness) and mounted using polyester resin. The deposition of conducting polymers on spontaneously passivating metals such as titanium and aluminum usually requires a pretreatment of the substrate in order to remove natural oxides, which cover the metal surface. Prior to electropolymerization of aniline, the titanium electrodes were first mechanically polished with different grades of abrasive

papers, rinsed in a run of distilled water, then chemically etched by immersing in a mixture of volumetric 1:4:5 of $HF:HNO_3:H_2O$. The last step of pretreatment was rinsed in distilled water. After the pretreatment, electropolymerization of aniline was conducted in 0.5 *M* H_2SO_4 solution containing of 0.1 *M* aniline + 0.0l and 0.015 g of g-C_3N_4 solution through 30 successive cyclic voltammetry (CV) scans in the potential range of −0.5 and 1.5 V at a scan rate of 10 mV s^{-1}. The temperature is maintained at 25 °C.

Characterization Techniques

Fourier transform infra-red (FTIR) spectra were recorded on Jasco-680 (Tokyo, Japan) spectrophotometer with 4 cm^{-1} resolution. The KBr pellet technique was applied for monitoring changes in the FTIR spectra of the samples in the range of 4000–400 cm^{-1}. The vibrational transition frequencies are reported in wavenumbers (cm^{-1}). X-ray diffraction (XRD) profiles were obtained with a Bruker (Rheinstetten, Germany) XRD (D8 Advance, Germany) advanced powder X-ray diffraction system at 45 kV and 100 mA. using Cu Ka radiation. The morphology of the hybrid was examined by transmission electron microscopy (TEM; Philips CM120 (Eindhoven, Netherlands)) and field emission scanning electron microscopy (FE-SEM; HITACHI S-4160 (Tokyo, Japan)) using an accelerator voltage of 100 kV. The UV–Vis absorption spectra were recorded using UV–vis–NIR spectrophotometer with an integrating sphere (DUV-3700, Shimadzu, Japan), which $BaSO_4$ was used as a reference. Electrochemical experiments were carried out using a computerized potentiostat/galvanostat (SAMA 500, Iran).

RESULTS AND DISCUSSION

Synthesis of PANI/g-C_3N_4 Hybrids

Nitrogen-rich g-C_3N_4 was synthesized from the stepwise condensation reaction of melamine and cyanuric chloride in the presence of *N*,*N*-dimethylmethanamide as a high boiling point nonnucleophilic base.[37] Due to the different reactivities of melamine and cyanuric chloride, the reaction was occurred at different temperatures. At low temperature (0 °C), only one site of triazine can be substituted, whereas two sites can participate in substitution reactions that occur at room temperature (25 °C), and all three sites can react under elevated temperatures (greater than 70 °C). Scheme 1 shows the step-wise formation of the g-C_3N_4 networks. The formation of g-C_3N_4 was confirmed by different techniques.

Cyclic Voltammetry

Cyclic voltammograms recorded during electropolymerization of PANI and PANI composites on titanium electrode in 0.5*M* H_2SO_4 solution containing of 0.1*M* aniline + 0.0l and 0.015 g of g-C_3N_4 solution at a scan rate of 10 mV s^{-1} are shown in Figure 1. Figure 1 shows CVs recorded during electropolymerization of PANI in the absence [Figure 1(a)] and in the presence of 0.0l g [Figure 1(b)] and 0.0l5 g [Figure 1(c)] of g-C_3N_4 solution. Upon the oxidation of its monomer, the PANI film starts to form and grow on the electrode surface as seen from its cyclic voltammogram. The oxidation and reduction peaks of the PANI film increase in intensity as the film grows. In the presence of g-C_3N_4, the increase in the peak intensities of the film is much faster. Also, with increasing cyclic numbers, shifts in

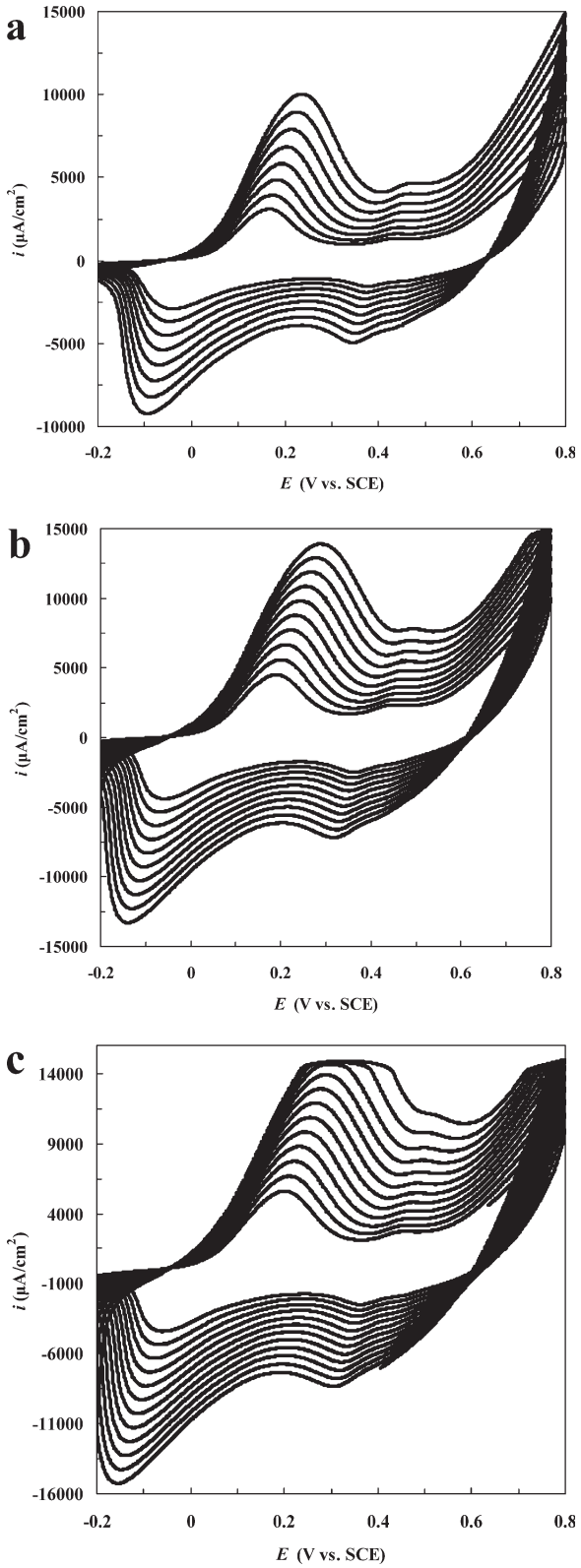

Figure 1. Cyclic voltammograms during polymerization in 0.5 *M* H_2SO_4 solution containing 0.1 *M* aniline at a scan rate of 10 mV s^{-1} (a) in the absence of g-C_3N_4, (b) in the presence of 0.010 g of g-C_3N_4, and (c) in the presence of 0.015 g of g-C_3N_4.

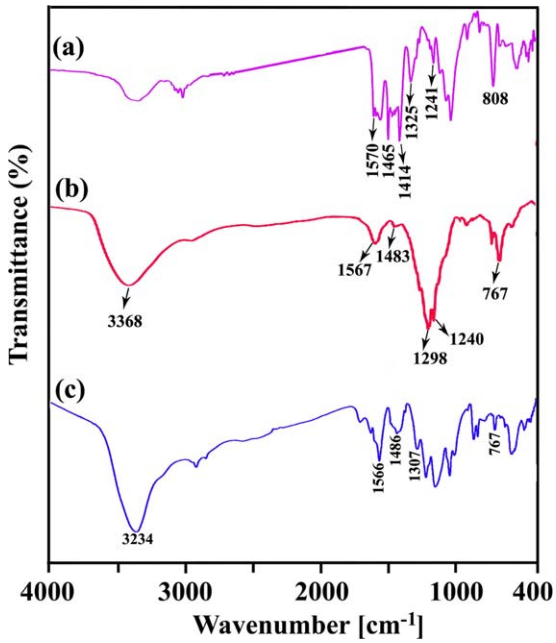

Figure 2. FTIR spectra of (a) g-C_3N_4, (b) pure PANI, and (c) PANI/g-C_3N_4 hybrids. [Color figure can be viewed in the online issue, which is available at wileyonlinelibrary.com.]

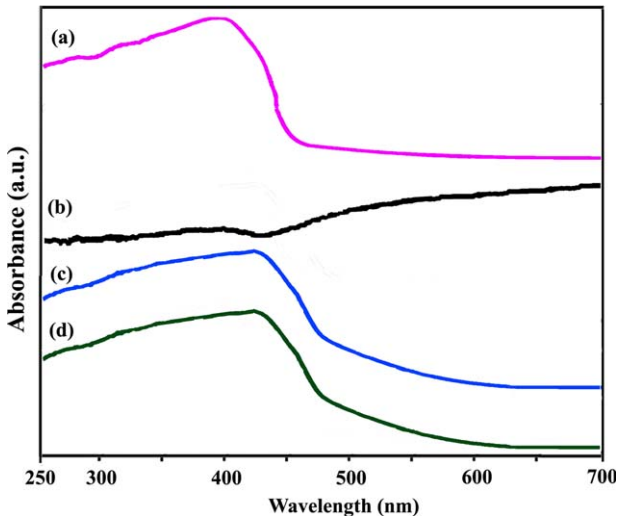

Figure 4. UV–vis diffuses reflection spectra of (a) g-C_3N_4, (b) PANI and PANI/g-C_3N_4 composite with (c) 0.01 g and (d) 0.015 g of g-C_3N_4. [Color figure can be viewed in the online issue, which is available at wileyonlinelibrary.com.]

the oxidation and reduction peak potentials can be seen. It seems that electrode kinetics changed by deposition and increased deposits on the surface of electrode. At the beginning, the electron transfer is between redox active species and the electrode surface (they pass through pin-holes, defects, etc.). But, by covering the electrode surface, they will block completely via electron transfer, and the shift of the oxidation and reduction peak potentials can be observed with increasing cyclic numbers.

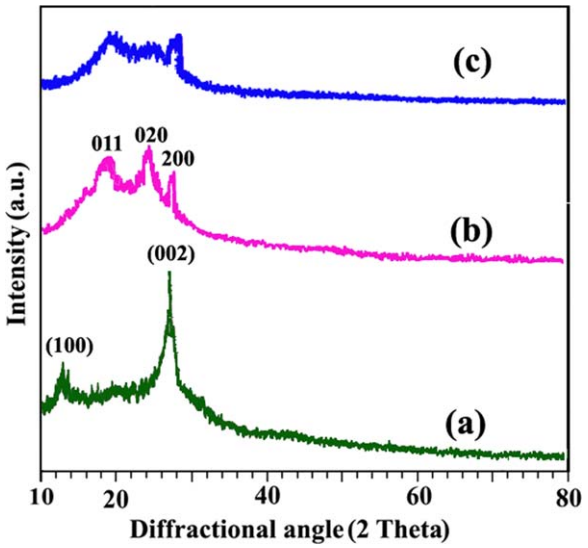

Figure 3. XRD pattern of (a) g-C_3N_4, (b) PANI, and (c) PANI/g-C_3N_4 composite. [Color figure can be viewed in the online issue, which is available at wileyonlinelibrary.com.]

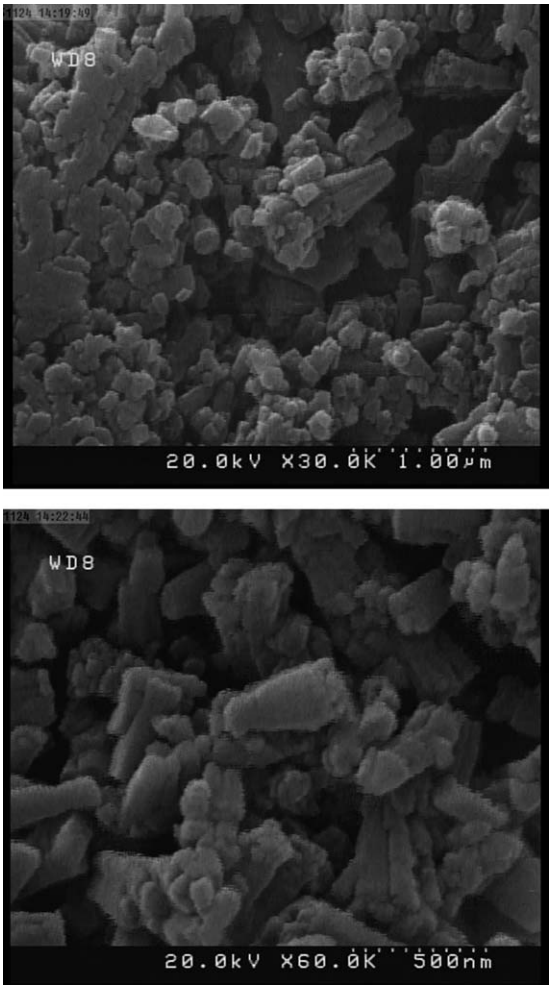

Figure 5. FE-SEM images of g-C_3N_4 with different magnifications.

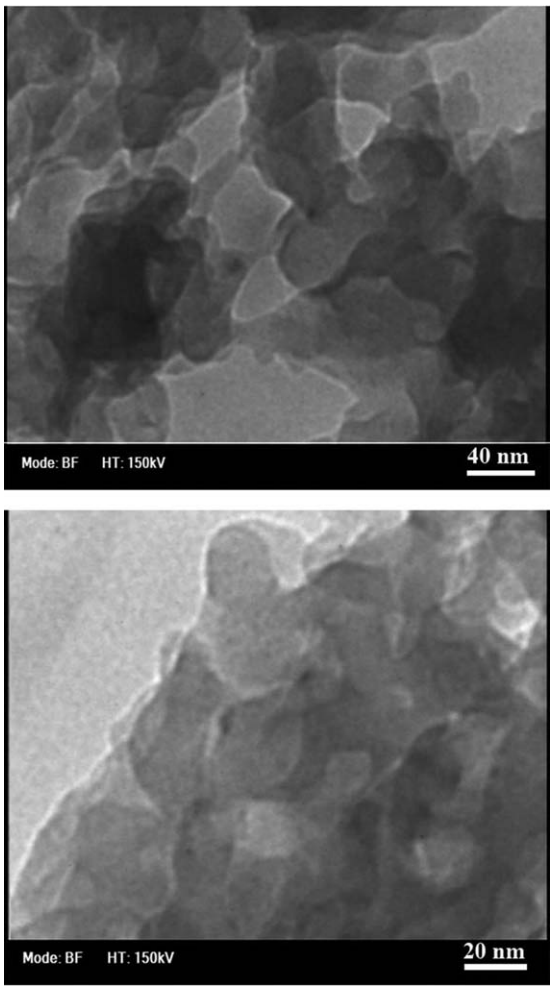

Figure 6. TEM images of g-C_3N_4 with different magnifications.

FTIR Study

The molecular structures of the synthesized g-C_3N_4, pure PANI, and hybrids of PANI/g-C_3N_4 are characterized by FTIR spectroscopy, and the results are presented in Figure 2. The spectrum of g-C_3N_4 nanostructures clearly shows several peaks at the frequency characteristic of vibrational modes related to the chemical bonding between carbon and nitrogen. The broad peak at 3000–3400 cm^{-1} is ascribed to the stretching vibration of N—H groups. The strong band of 1200–1600 cm^{-1}, with the characteristic peaks at 1241, 1325, 1414, 1465, and 1570 cm^{-1}, is attributed to the typical stretching vibration of C—N and C═N heterocycles [Figure 2(a)]. The characteristic peak at 808 cm^{-1} was assigned to the breathing mode of triazine units.[38,39] Figure 2(b) shows the FTIR spectra of the pristine PANI which was produced by electropolymerization of aniline monomer. The characteristic peak at 3368 cm^{-1} can be attributed to the hydrogen bonding between N—H of amine and imine sites [Figure 2(b)]. The C═N and C═N stretching of the quinonoid and benzenoid rings was appeared at 1562 and 1481 cm^{-1}. The bands at 1302 and 1240 cm^{-1} were ascribed to the C—N stretching mode for the benzenoid unit, while the band at 1111 cm^{-1} to the quinonoid unit of PANI and the peak at 767 cm^{-1} are associated with C—C and C—H in the benzenoid unit.[40]

For the hybrid of PANI and g-C_3N_4, the major peaks of both PANI and g-C_3N_4 were observed as shown in Figure 2(c). Though, some differences from either PANI or g-C_3N_4 are observed. For instance, the PANI/g-C_3N_4 reveals a band at 767 cm^{-1}, which is attributed to the out-of-plane bending vibrations of C—H band in the aromatic ring. However, it became weak after doping, because the PANI chain was anchored by the g-C_3N_4 plane, and aromatic structures were conjugated with the g-C_3N_4 plane via π-stacking. The out-of-plane bending vibrations were restricted naturally. For the PANI/g-C_3N_4 sample, the characteristic peaks from PANI around 1302, 1481, and 1562 cm^{-1} shift to higher wave numbers of 1307, 1486 and 1566 cm^{-1} after the g-C_3N_4 are introduced. Meanwhile, the hydrogen bond absorption at 3234 cm^{-1} is strengthened. These results suggested that not only the PANI/g-C_3N_4 has main chain of the PANI, but also the PANI is loaded with g-C_3N_4 as the dopant.

X-ray Diffraction Study

The X-ray diffraction patterns of the as-prepared samples are shown in Figure 3. The detailed information on the purity and crystallinity of the samples was obtained in the XRD measurement. Figure 3 shows the XRD patterns of the g-C_3N_4, PANI,

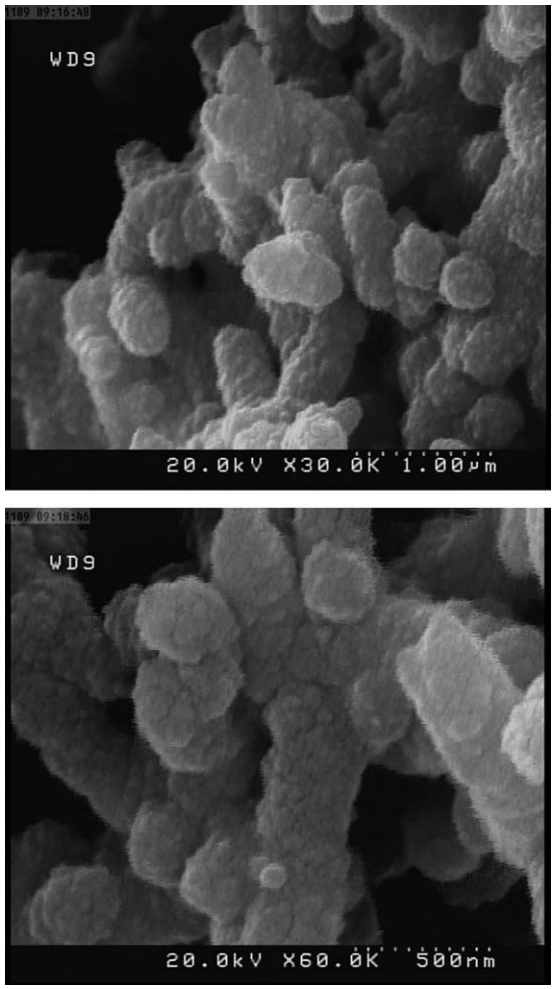

Figure 7. FE-SEM images of as-synthesized PANI with different magnifications.

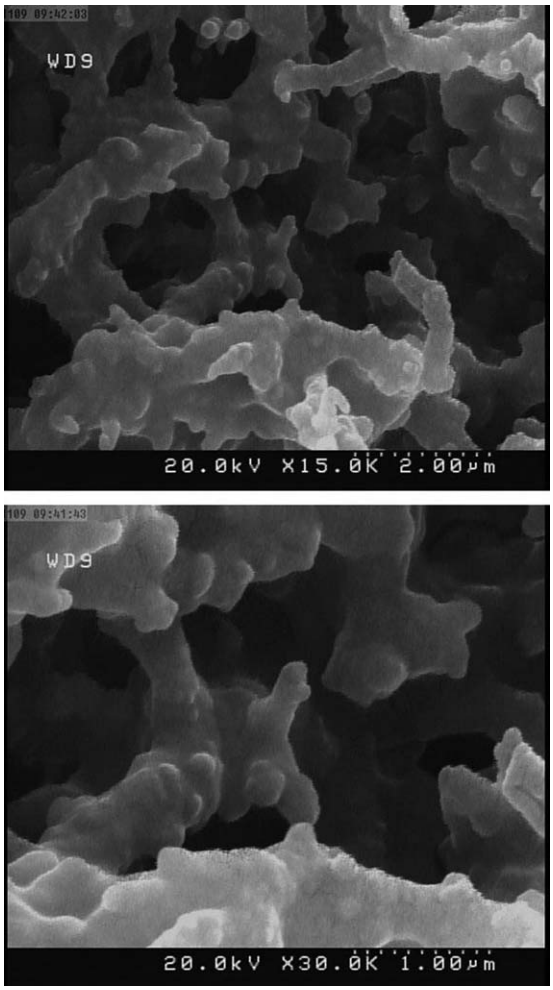

Figure 8. FE-SEM images of PANI/g-C_3N_4 composite with 0.01 g of g-C_3N_4.

and PANI/g-C_3N_4 composites. For pure g-C_3N_4 sample [Figure 3(a)], the characteristic peaks at 27.4 and 12.6° correspond to the (002) plane arising from the stacking of the conjugated aromatic system and the (100) plane diffraction arising from the in-plane repeating motifs of the continuous heptazine network, respectively.[41] In the XRD patterns of PANI, the characteristic peaks appeared at 15.8, 20.5, and 26.3° corresponding to (011), (020), and (200) crystal planes, respectively.[42] The peak at 15.8° is attributed to parallel repeat units of PANI. The peak at 20.5° is usually ascribed to the periodicity parallel and perpendicular to the polymer chains of PANI, as well as the peak at 26.3° is assigned to a periodicity caused by H-bonding between PANI chains [Figure 3(b)]. When g-C_3N_4 was incorporated into the PANI matrix, the diffraction peak of g-C_3N_4 at 26.3° was overlap with the peak of PANI, which results in the broad and intense peak in the composite [Figure 3(c)]. The data indicate that no additional crystalline order has been introduced into the composite. Compared with functionalized g-C_3N_4, the obvious characteristic peaks in PANI/g-C_3N_4 hybrids can be ascribed to the formation of crystal appearing on the outer layers of g-C_3N_4. This result shows that the homogeneous coating of PANI onto the g-C_3N_4 indicates that it was well dispersed in polymer matrix.

Absorbance Properties

The absorbance properties of the synthesized materials were measured using UV–vis diffuse reflectance spectroscopy. As illustrated in Figure 4(a), the pure g-C_3N_4 sample can absorb both UV and visible light with an absorption edge at 460 nm, which can be assigned to the intrinsic band gap of g-C_3N_4 (2.7 eV).[43,44] Pristine PANI can not only absorb UV light but also has strong absorption in visible light and near infrared regions, which can be attributed to transitions in the PANI molecules.[45] A comparison of the absorption spectra of the pure g-C_3N_4 with those acquired from the PANI/g-C_3N_4 shows that the composites exhibit stronger absorption in the visible region at wavelengths longer than 400 nm, and the red shifts are also observed in the composite samples after the *in situ* formation of PANI polymers (Figure 4).

Morphological Study

The morphology and microstructure of the samples were investigated by FE-SEM and transmission electron microscopy (TEM) techniques. FE-SEM images [Figure 5(a,b)] show that g-

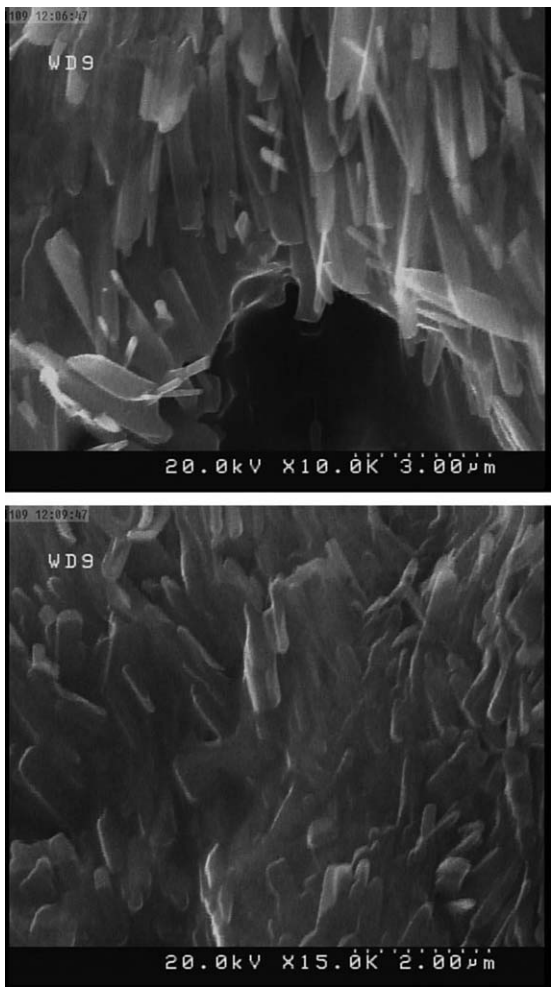

Figure 9. FE-SEM images of PANI/g-C_3N_4 composite with 0.015 g of g-C_3N_4.

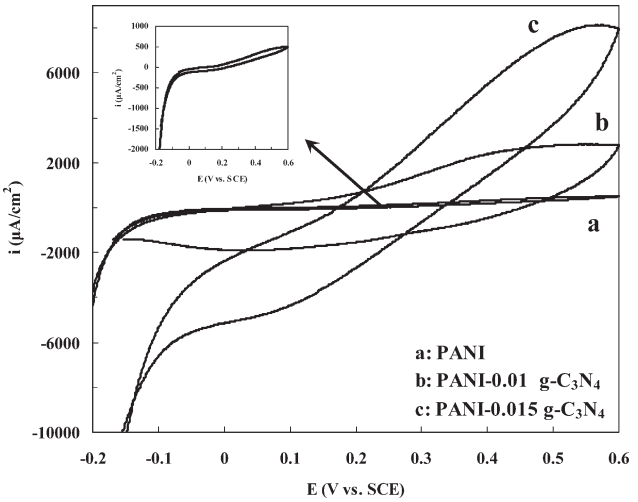

Figure 10. Cyclic voltammograms of various samples in 1*M* H_2SO_4 at the scan rate of 10 mV s^{-1}: (a) PANI, (b) PANI–0.01 g of g-C_3N_4, and (c) PANI–0.015 g of g-C_3N_4.

C_3N_4 has random stacking clubbed morphology with anomalous smooth nanostructure. Figure 6 shows the TEM image of the g-C_3N_4. According to the TEM images, the g-C_3N_4 shows its characteristic platelet-like, layered morphology (Figure 6).

The structure and morphology of the pristine PANI and PANI/g-C_3N_4 composites with 0.01 and 0.015 g of g-C_3N_4 was investigated by FE-SEM techniques with different magnifications. As shown in Figure 7, the pure PANI formed flake-like agglomerations, which were stacked by spherical particles. When g-C_3N_4 was incorporated to the polymer, the g-C_3N_4 nanosheets were dispersed on the surface of PANI and tended to exist in the form of small nanosheets. In the case of PANI/g-C_3N_4 composites with 0.01 g of g-C_3N_4, the resulting hybrids show spherical particles in which g-C_3N_4 particles get deposited on the surface of PANI and get the composite structures (Figure 8). By increasing the amount of g-C_3N_4 in the PANI/g-C_3N_4 composites (sample with 0.015 g of g-C_3N_4), the hybrids show road-like morphology (Figure 9).

Electrochemical Performance

The capacitive performance of the PANI and PANI/g-C_3N_4 composite films is evaluated by CV tests. Figure 10 shows the cyclic voltammograms of various samples, recorded in 0.5 *M* H_2SO_4 electrolyte with the potential scan rate of 10 mV s^{-1} at the potential range −0.20–0.60 V. Voltammograms are the same in shape except in the capacitance of the PANI/g-C_3N_4 composite films electrode became larger than that of PANI film electrode at the same scan rate. The higher capacitance of films may be attributed to the larger surface area of these samples in comparison to the neat polymer. This results in more interfacial surface between the nanostructures and the electrolyte, leading to more fascinated reactions.

CONCLUSIONS

PANI/g-C_3N_4 composite films with different contents of g-C_3N_4 on the titanium substrate were synthesized by a versatile and facile electropolymerization method. XRD, FE-SEM, EDX, and FTIR have been used to characterize these films. FE-SEM images showed that PANI intercalated into g-C_3N_4 sheets and coated on the surface of titanium homogeneously. The prepared samples were investigated as supercapacitor electrode materials in 0.5*M* H_2SO_4 as the electrolyte solution using CV. As compared to the PANI film, the PANI/g-C_3N_4 composite film has a higher specific capacitance.

REFERENCES

1. Salvatore Arico, A.; Bruce, P.; Scrosati, B.; Tarascon, J.; Van Schalkwijk, W. *Nat. Mater.* **2005**, *4*, 366.
2. Zhou, G. M.; Li, F.; Cheng, H. M. *Energy Environ. Sci.* **2014**, *7*, 1307.
3. Nyholm, L.; Nystrom, G.; Mihranyan, A.; Stromme, M. *Adv. Mater.* **2011**, *23*, 3751.
4. Yu, M.; Qiu, W.; Wang, F.; Zhai, T.; Fang, P.; Lu, X.; Tong, Y. *J. Mater. Chem. A* **2015**, *3*, 15792.
5. Xie, Y.; Xia, C.; Du, H.; Wang, W. *J. Power Sources* **2015**, *286*, 561.
6. Yu, A.; Chabot, V.; Zhang, J. Electrochemical Supercapacitors for Energy Storage and Delivery: Fundamentals and Applications. CRC Press/Taylor & Francis Group; NJ, USA, **2013**.
7. Khosrozadeh, A.; Xing, M.; Wang, Q. *Appl. Energy* **2015**, *153*, 87.
8. Chen, Y.; Zhang, X.; Xie, Z. *ACS Nano* **2015**, *9*, 8054.
9. Shi, F.; Li, L.; Wang, X. L.; Gu, C. D.; Tu, J. P. *RSC Adv.* **2014**, *4*, 41910.
10. Xiong, P.; Zhu, J.; Wang, X. *J. Power Sources* **2015**, *294*, 31.
11. Lu, X. H.; Yu, M. H.; Wang, G. M.; Zhai, T.; Xie, S. L.; Ling, Y. C.; Tong, Y. X.; Li, Y. *Adv. Mater.* **2013**, *25*, 267.
12. Deng, Y.; Xie, Y.; Zou, K.; Ji, X. *J. Mater. Chem. A* **2015**, *4*, 1144.
13. Ding, S. D.; Bhargava, X.; Kourkoutis, A.; Robinson, L. F. *Chem. Mater.* **2015**, *27*, 7861.
14. Li, Z.; Ma, G.; Ge, R.; Huo, K.; Zhou, Y. *Angew. Chem. Int. Ed.* **2016**, *55*, 979.
15. Gurunathan, K.; Murugan, A. V.; Marimuthu, R.; Mulik, U. P.; Amalnerkar, D. P. *Mater. Chem. Phys.* **1999**, *61*, 173.
16. Potphode, D. D.; Sivaraman, P.; Mishra, S. P.; Patri, M. *Electrochim. Acta* **2015**, *155*, 402.
17. Kaur, B.; Srivastava, R. A. *New J. Chem.* **2015**, *39*, 6899.
18. Yang, L.; Tang, Y.; Yan, D.; Liu, C.; Luo, S. *ACS Appl. Mater. Int.* **2016**, *8*, 169.
19. Canales, M.; Torras, J.; Fabregat, G.; Meneguzzi, A.; Alemán, C. *J. Phys. Chem. B* **2014**, *118*, 11552.
20. Wang, K.; Wu, H. P.; Meng, Y. N.; Wei, Z. X. *Small* **2014**, *10*, 14.
21. Zhu, S.; Wu, M.; Ge, M. H.; Zhang, S. K.; Li, C. H. *J. Power Sources* **2016**, *306*, 593.
22. Wang, X.; Maeda, K.; Chen, X.; Takanabe, K.; Domen, K.; Hou, Y.; Fu, X.; Antonietti, M. *J. Am. Chem. Soc.* **2009**, *131*, 1680.

23. Chen, Q.; Zhao, Y.; Huang, X.; Chen, N.; Qu, L. *J. Mater. Chem. A* **2015**, *3*, 6761.
24. Dong, X.; Cheng, F. *J. Mater. Chem. A* **2015**, *3*, 23642.
25. Shi, L.; Zhang, J.; Liu, H.; Que, M.; Cai, X.; Tan, S. *Mater. Lett.* **2015**, *145*, 150.
26. Zhang, L.; Ou, M.; Yao, H.; Li, Z.; Qu, D.; Liu, F.; Wang, J.; Wang, J.; Li, Z. *Electrochim. Acta* **2015**, *186*, 292.
27. Zheng, Y.; Jiao, Y.; Chen, J.; Liu, J.; Liang, J.; Du, A.; Zhang, W.; Zhu, Z.; Smith, S. C.; Jaroniec, M.; Lu, G. Q.; Qiao, S. Z. *J. Am. Chem. Soc.* **2011**, *133*, 20116.
28. Tahir, M.; Cao, C. B.; Mahmood, N.; Butt, F. K.; Mahmood, A.; Idrees, F.; Hussain, S.; Tanveer, M.; Ali, Z.; Aslam, I.; Multifunctional, g-CN4.; Nanofibers, A. *ACS Appl. Mater. Interfaces* **2014**, *6*, 1258.
29. She, X.; Xu, H.; Wang, H.; Du, D.; Li, H. *Dalton Trans.* **2015**, *44*, 7021.
30. Wang, K.; Li, Q.; Liu, B.; Ho, W.; Yu, J. *Appl. Catal. B: Environ.* **2015**, *176–177*, 44.
31. Chen, Y.; Lin, B.; Wang, H.; Yang, Y.; Zhu, H.; Yu, W.; Basset, J. *Chem. Eng. J.* **2016**, *286*, 339.
32. Luo, W. B.; Chou, S. L.; Wang, J. Z.; Zhai, Y. C.; Liu, H. K. *Small* **2015**, *11*, 2817.
33. Bai, S.; Wang, X.; Hu, C.; Jiang, J.; Xiong, Y. *Chem. Commun.* **2014**, *50*, 6094.
34. Dong, F.; Ni, Z.; Li, P.; Wu, Z. *New J. Chem.* **2015**, *39*, 4737.
35. Liu, C.; Huang, H.; Du, X.; Guo, Y.; Zhang, Y. *J. Phys. Chem. C* **2015**, *119*, 17156.
36. Zhang, M.; Jiang, W.; Liu, D.; Zhu, Y.; Zhu, Y. *Appl. Catal. B* **2016**, *183*, 263.
37. Kim, O. H.; Cho, Y. H.; Chung, D. Y.; Kim, M. J.; Yoo, J. M.; Park, J. E.; Choe, H.; Sung, Y. E. *Sci. Rep.* **2015**, *5*, 1. Article number: 8376
38. Dong, F.; Wu, L.; Sun, Y. J.; Fu, M.; Wu, Z. B.; Lee, S. C. *J. Mater. Chem.* **2011**, *21*, 15171.
39. Li, Y. B.; Zhang, H. M.; Liu, P.; Wang, D.; Li, Y.; Zhao, H. J. *Small* **2013**, *9*, 3336.
40. Dinari, M.; Momeni, M. M.; Goudarzirad, M. *J. Mater. Sci.* **2016**, *51*, 2964.
41. Sun, J. H.; Zhang, J. S.; Zhang, M. W.; Antonietti, M.; Fu, X. Z.; Wang, X. C. *Nat. Commun.* **2012**, *2*, 1139.
42. Dinari, M.; Momeni, M. M.; Goudarzirad, M. *Sur. Eng.*, **2016**, *35*, 535.
43. Tian, N.; Huang, H.; He, Y.; Guo, Y.; Zhang, Y.; Novel g, C. N. *RSC Adv.* **2014**, *4*, 42716.
44. Huang, Z.; Sun, Q.; Lv, K.; Zhang, Z.; Li, M.; Li, B. *Appl. Cat. B: Environ.* **2015**, *164*, 420.
45. Ge, L.; Han, C.; Liu, J. *J. Mater. Chem.* **2012**, *22*, 11843.